




Enhancement in photovoltaic properties of Nd:SnS films prepared by low-cost NSP method

S. Sebastian* , I. Kulandaisamy, A. M. S. Arulanantham, S. Valanarasu, A. Kathalingam, Mohd. Shkir, Salem AlFaify

Received: 17 September 2018 / Revised: 24 November 2018 / Accepted: 7 May 2019 / Published online: 20 July 2019
© The Nonferrous Metals Society of China and Springer-Verlag GmbH Germany, part of Springer Nature 2019

Abstract The inner transition metal (ITM) neodymium (Nd)-doped tin sulfide (Nd:SnS) thin films with various Nd concentrations were coated by nebulizer spray pyrolysis (NSP) technique at 350 °C. All the coated films were analyzed for their structural, optical and photoelectrical properties. X-ray diffractometer (XRD) study showed (111) direction as the highly preferred orientation with orthorhombic crystal structure for all the films. The intensity of the peaks was found to increase until 5 at% Nd doping and then reduced for higher (7 at% Nd) doping concentration. Atomic force microscopic (AFM) images of the films proclaimed an increase in the surface and line roughness of the films by increasing Nd concentrations. Optical analysis on the films showed a variation in energy gap from 2.05 to 1.69 eV when the doping concentration increased from 0 at% to 7 at%. At 5 at% Nd doping, the photoluminescence (PL) spectra displayed a single strong emission peak at 723.1 nm with enhanced intensity corresponding to near-band-edge emission. All the SnS thin films exhibited p-type behavior with the lowest resistivity of $\sim 4.311 \Omega\text{-cm}$ and high carrier concentrations

of $\sim 1.441 \times 10^{17} \text{ cm}^{-3}$ for 5 at% Nd doping level as observed from Hall effect studies. Furthermore, fluorine-doped tin oxide (FTO)/n-CdS/p-Nd:SnS hetero-junction solar cells were prepared and the current–voltage curve in dark and light condition was obtained for the device. An efficiency of 0.135% was observed for the solar cell fabricated with 5 at% Nd-doped SnS thin film.

Keywords Rare earth doping; Neodymium; SnS thin films; Nebulizer spray; Optical studies; Solar cells

1 Introduction

Tin sulfide (SnS), a semiconductor compound, classified as IV–VI group, has good electro-optical stuff for solar cells [1]. It has orthorhombic crystal structure, p-type electrical conductivity [2] and high absorption coefficient greater than $1 \times 10^4 \text{ cm}^{-1}$ [3]. These properties make it an excellent light-absorbing material to manufacture hetero-junction solar cells. The elemental constituents of SnS are also non-toxic, cheap and adequate in nature, and these are the added advantages of this material. Deposition of SnS films could be done by many methods, such as vacuum evaporation [1], chemical bath deposition (CBD) [4], dip deposition [5], rf-sputtering [6] and spray pyrolysis [7]. Among all the methods, the nebulizer spray pyrolysis (NSP) method is a feasible technique which can give films of uniform deposits without pinholes in required thickness with large area at low cost [8]. For a potential photovoltaic cell, the absorber layer should have an optimal energy gap (E_g) and high absorption (α) coefficient [9]. As tin sulfide has these properties, it can suitably be used in solar cells.

The electrical conductivity of p-type SnS materials can be controlled by doping the elements such as Al, Cl, Sb, N

S. Sebastian*, I. Kulandaisamy, A. M. S. Arulanantham, S. Valanarasu
PG & Research Department of Physics, Arul Anandar College, Karumathur, Madurai 625 514, India
e-mail: speedseba@yahoo.co.in

A. Kathalingam
Millimeter Wave Innovation Technology Research Center (MINT), Dongguk University-Seoul, Seoul 04620, Republic of Korea

Mohd. Shkir, S. AlFaify
Advanced Functional Materials & Optoelectronics Laboratory (AFMOL), Department of Physics, Faculty of Science, King Khalid University, Abha 9004, Saudi Arabia

and Ag [10, 11], whereas the physical properties of SnS materials can be enhanced by adding Se [12], Bi [13], Fe [14], Ag [15], In [16] and Cu [17] as dopants. From our literature survey, we did not find any reports on Nd-doped SnS thin films. Hence, in this work, we prepared Nd:SnS films through NSP method and characterized to see the persuasion of Nd dopant on key optoelectronic properties chattels. The systematic investigation of dopant concentration variation on the various physical characteristics of SnS films was reported.

2 Experimental

2.1 Materials and methods

Analytical reagent (AR)-grade tin (IV) chloride ($\text{SnCl}_2 \cdot 2\text{H}_2\text{O}$), thiourea ($\text{CS}(\text{NH}_2)_2$) and neodymium (III) acetate ($\text{Nd}(\text{O}_2\text{C}_3\text{H}_3)_3 \cdot x\text{H}_2\text{O}$) were used as starting materials for tin, sulfur and neodymium precursors, respectively, to prepare Nd-doped and undoped SnS thin films on glass substrate. Blue star soda lime glass substrates were systematically cleaned and used to deposit the films. A 3:1 molar ratio proportion of tin and thiourea was liquefied in 10 ml of distilled water, in which few drops of HCl were also added for total solubility of the salts. In the nebulizer, spray-condensed air was preferred as a gas hauler for the formation of fumes. Keeping the substrate temperature at $(350 \pm 5)^\circ\text{C}$ accuracy, the prepared solution was sprayed onto the substrate. For the preparation of Nd-doped films, different concentrations of neodymium (III) acetate (1 at%, 3 at%, 5 at% and 7 at%) were used. The substrate-to-spray nozzle distance was set at 50 mm. After spraying the solution, the substrate was left to cool down to room condition, and then, the prepared SnS films were removed from the heater and taken to various characterization studies. CdS film was also prepared in the same manner using the precursors cadmium chloride and thiourea at 310°C .

2.2 Characterization techniques

The thickness of the prepared SnS thin films was measured using a stylus profilometer. X-ray diffractometer (XRD, JEOL JDX—803) was used to examine the structural properties of pristine and Nd-added SnS films. For this XRD characterization, the prepared samples were scanned in the steps of $0.02^\circ \cdot \text{min}^{-1}$ in the 2θ range of 10° – 80° continuously. Princeton Acton SP 2500 Raman instrument was used at room temperature for the structural identification of the films. The surface topography and roughness of the films were visualized by atomic force microscopy (AFM, Nanosurf Easyscan 2 static mode). Optical

properties were measured by an ultraviolet–visible (UV–Vis) spectrometer in the wavelength range of 350–900 nm. Photoluminescence (PL) spectrum of the samples was obtained using a spectrofluorometer at room temperature using 350-nm wavelength of excitation. Four-probe Hall effect instrument was used to study the electrical properties. Keithley source meter with $100 \text{ mW} \cdot \text{cm}^{-2}$ illumination was employed to record the variation of current density and voltage (J – V) of the prepared solar cells using p-type Nd-doped SnS films. For optical illumination, the solar cell light was focused onto the fluorine-doped tin oxide (FTO) glass side.

3 Results and discussion

3.1 XRD analysis

Figure 1 illustrates XRD patterns of inner transition metal neodymium (Nd)-doped tin sulfide (Nd:SnS) thin films coated with different Nd concentrations (0 at% to 7 at%) on glass substrate at 350°C . It confirms the polycrystalline nature of the coated films according to the JCPDS card No. 075-2115 of SnS. Irrespective of the difference in Nd doping concentration, all the films displayed a major peak along (111) plane, indicating the most favored orientation and phase purity of SnS. A similar single phase of crystalline SnS films was reported using a chemical spray

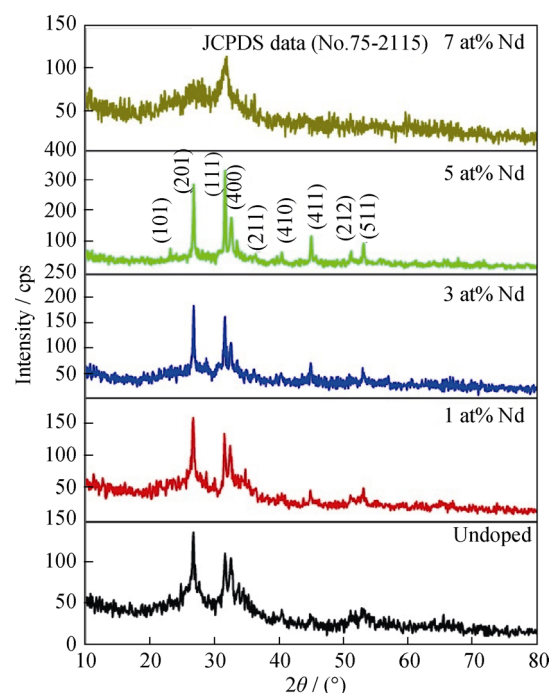


Fig. 1 XRD patterns of undoped and Nd-doped SnS films with different Nd doping contents

method [18] and CBD method [19]. As the doping concentration increases from 0 at% to 5 at%, the intensity of the orientated peak also increases, which might be due to the reduction in stress in deposited films doped with higher ionic radius element Nd³⁺ (0.0995 nm) than that of Sn²⁺ (0.0930 nm) [16]. No detection of impurities or other neodymium (Nd)-related peaks is seen in XRD measurement.

Since the ionic radius of Sn²⁺ (0.0930 nm) is lower than that of Nd³⁺ (0.0995 nm), the substitutional incorporation of Nd³⁺ in SnS induces notable changes in crystalline size and lattice constant [20]. The lattice distance (*d_{hkl}*) between the adjacent planes increases when a higher-radius ionic element is substituted with a lower-radius ionic element. The valence state difference and its adverse effects of Sn²⁺ and Nd³⁺ were also previously reported in Al-doped SnS [20] and Cu-doped SnS [21]. Hence, the extra Nd atoms incorporated at interstitial sites for higher Nd doping concentration (5 at%) lead to the lattice expansion.

The size of crystallites (*D*), dislocation density (*δ*), microstrain (*ε*), number of crystallites (*n_c*) and a texture coefficient (*TC_(hkl)*) calculated using Scherrer's relations [17, 22] are summarized in Table 1.

$$D = \frac{0.9\lambda}{\beta \cos \theta} \tag{1}$$

$$\delta = \frac{1}{D^2} \tag{2}$$

$$\epsilon = \frac{\beta \cos \theta}{4} \tag{3}$$

$$n_c = \frac{t}{D^3} \tag{4}$$

$$TC_{(hkl)} = \frac{I_{(hkl)}/I_{0(hkl)}}{\frac{1}{n} \sum I_{(hkl)}/I_{0(hkl)}} \tag{5}$$

where *k* is shape factor (*k* = 0.9), *λ* is wavelength (*λ* = 0.15406 nm), *β* is full width at half maximum (FWHM), *θ* is Bragg's angle, *t* is thickness, *I_(hkl)* is standard intensity, *I_{0(hkl)}* is measured intensity and *n* is reflection number. The crystallite size (*D*) is found to increase from 17 to 41 nm when Nd doping concentration

increases from 0 at% to 5 at%, as shown in Table 1. Crystallinity of the films is enhanced by increasing Nd doping concentration from 0 at% to 5 at% because of the regular arrangements of atoms in the crystal lattice. With further increase in doping concentration to 7 at%, the crystalline size decreases to 10 nm because of the increase in dislocation density, strain and number of crystallites. This result attributes to the adverse effect of higher doping concentration on new nucleation, leading to poor crystallinity of the film for 7 at% Nd doping [17, 23]. The crystallite size variation may also be due to lattice dilatation of SnS. This similar effect was also published by Damian et al. [24]. The *δ*, *ε*, *n_c* and *TC* values of films calculated using the above relations decrease progressively as the concentration of Nd doping increases, as shown in Table 1. The increase in Nd doping concentration from 0 at% to 5 at% results in the enhancement in regular arrangements of atoms in the crystal lattice. For further increase in doping concentration from 5 at% to 7 at%, the *δ*, *ε* and *n_c* values are enhanced. These outcomes feature the adverse effect of increase in doping concentration (> 5 at%) on the crystalline quality deterioration of the films [25].

3.2 Raman analysis

The chemical and structural information of the prepared Nd-doped SnS materials was examined using Raman instrument in the wavenumber range of 0–500 cm⁻¹. The Raman spectra obtained on the surface of the film as well as from the spots are given in Fig. 2. The SnS materials with orthorhombic crystal structure basically have 24 vibrational modes. The vibrational modes at the center of Brillouin zone could be specified as:

$$\Gamma = 4A_g + 2B_{1g} + 4B_{2g} + 2B_{3g} + 2A_u + 4B_{1u} + 2B_{2u} + 4B_{3u} \tag{6}$$

Among the 21 phonon modes, two (2A_u) are inactive modes, 12 (4A_g, 2B_{1g}, 4B_{2g} and 2B_{3g}) are Raman-active

Table 1 Microstructural parameters of undoped and Nd-doped SnS thin films

Nd doping content/at%	2θ/(°)	FWHM/(°)	Crystallite size/nm	Dislocation density/(10 ¹⁵ lines·m ⁻²)	Microstrain/(10 ⁻³ lines ² ·m ⁻⁴)	Number of crystallites/(10 ¹⁷ lines·m ⁻²)	Texture coefficient	Thickness/nm
0	31.5714	0.4920	17	3.6350	2.059	1.53	1.091	750
1	31.5712	0.3436	24	1.7730	1.438	0.57	1.117	785
3	31.5864	0.2562	32	0.9860	1.072	0.53	1.138	830
5	31.5851	0.1998	41	0.5995	0.837	0.13	1.279	870
7	31.6040	0.8400	10	10.5960	3.516	7.23	1.032	723

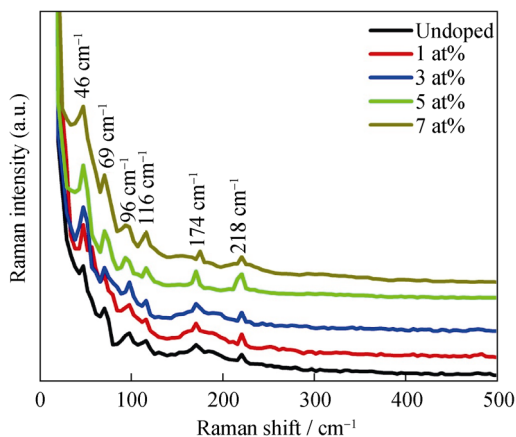


Fig. 2 Raman spectra of undoped and Nd-doped SnS with different Nd doping contents

modes, and seven ($3B_{1u}$, $1B_{2u}$ and $3B_{3u}$) are infrared-active modes [26]. The observed Raman emissions at 46, 69, 96, 116, 174 and 218 cm^{-1} are associated with the SnS optical phonon modes which agree with the earlier report by Srinivasa et al. [27]. The availability of various modes is due to the collision and scattering of light and even by the electrical polarization induced due to the scattered and incident photons [28]. Raman emission at 96 cm^{-1} is related to transverse optical mode A_g (TO), whereas the

longitudinal optical mode A_g (LO) is found at 218 cm^{-1} . Also, the emissions at 46, 174 and 69 cm^{-1} are allocated to B_{3g} and B_{2g} or B_{1g} modes [29]. This Raman result confirms the formation of SnS thin films without any impurities such as SnS_2 and Sn_2S_3 whose intense peaks are roughly at 308 and 312 cm^{-1} , respectively [30].

3.3 Micrograph and compositional analysis

Morphology of the films was characterized by AFM in $6\text{ }\mu\text{m} \times 6\text{ }\mu\text{m}$ area for two-dimensional (2D) and three-dimensional (3D) images; the surface topography of the films is shown in Fig. 3a–e. It illustrates the 2D and 3D AFM micrographs of SnS films of various Nd (0 at%, 1 at%, 3 at%, 5 at% and 7 at%) doping concentrations. The figures of pure SnS films illustrate the clear and smaller triangular-shaped grains with a larger number of grain boundaries displaying sand-like structure. The substrate's surface has a complete coverage with island-type arrangements. The increase in Nd doping concentration from 0 at% to 5 at% increases the surface roughness and grain size, showing uniform coverage on films surface. It is observed that the 0 at% doped film surface roughness value is about 7 nm and the grain size is 23 nm. But, the incorporation of Nd ions into the SnS films attributes an increase in grain size, as shown in Table 2. This similar effect of

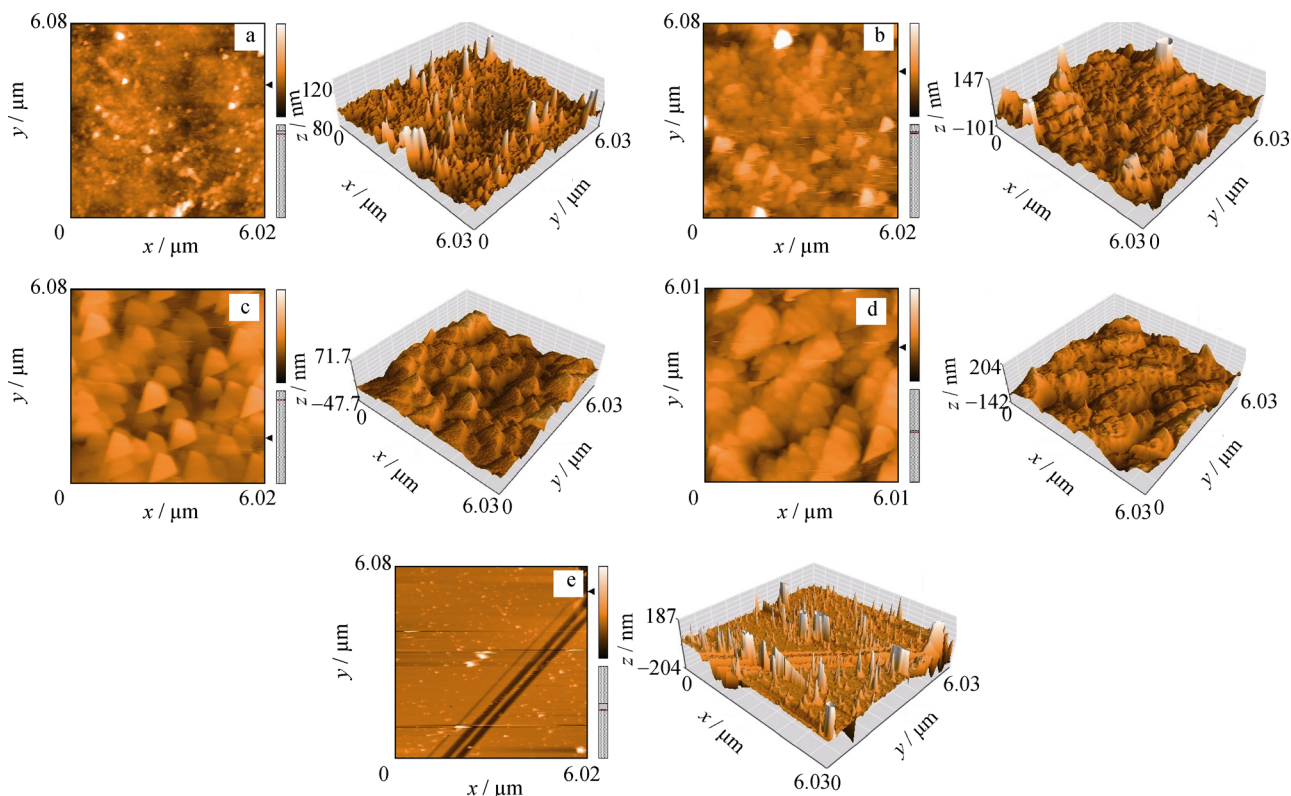
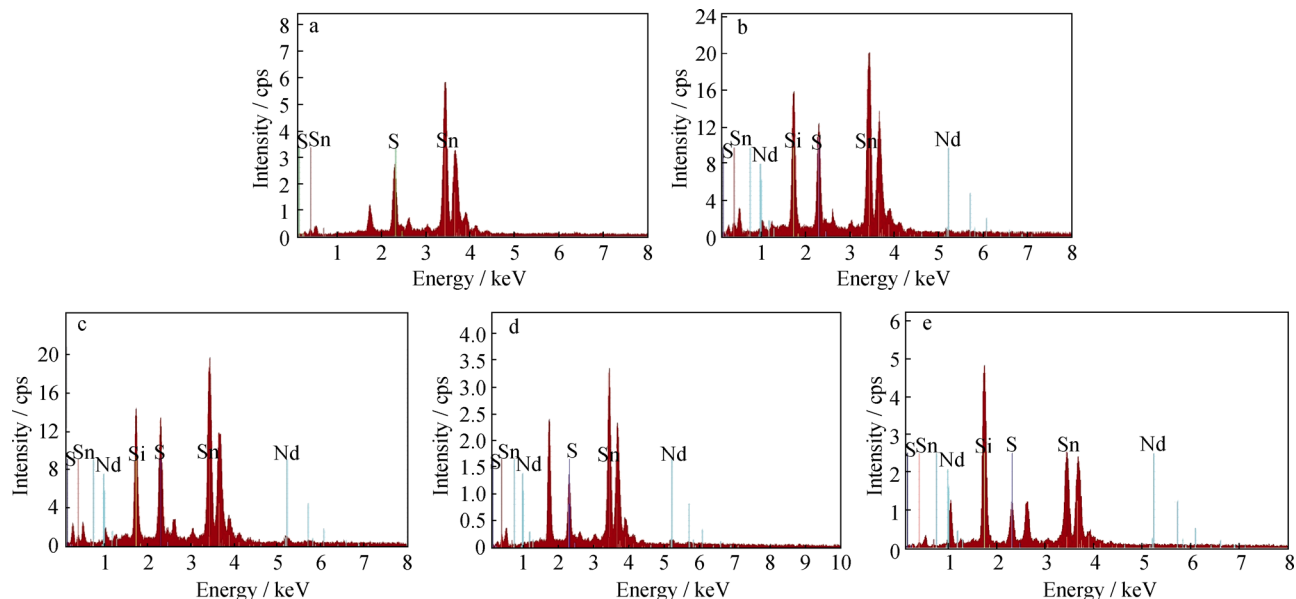


Fig. 3 2D and 3D AFM images of undoped and Nd-doped SnS thin films: **a** 0 at%, **b** 1 at%, **c** 3 at%, **d** 5 at% and **e** 7 at%

Table 2 Surface area, grain size and energy gap values of undoped and Nd-doped SnS thin films

Nd doping content/at%	Surface roughness/nm	Grain size/nm	Energy gap/eV
0	7	23	2.01
1	11	37	1.89
3	21	43	1.82
5	32	59	1.69
7	5	18	2.05

**Fig. 4** EDX spectra of undoped and Nd-doped SnS thin films: **a** 0 at%, **b** 1 at%, **c** 3 at%, **d** 5 at% and **e** 7 at%

roughness increase for bismuth-doped SnS film was also observed previously [31]. The same increasing trend of roughness with Sb-doped SnS [32] thin films has been already reported. It is evident that the size of the grain increases with the rise in Nd doping concentrations. With the further increase in doping concentration to 7 at%, the particle size of films decreases, as seen in Table 1. Moreover, the doped films are found to be denser with large number of uniform triangular granular grains. The increase in roughness of 5 at% Nd-doped sample indicates the merge of smaller grains, forming bigger grains, increasing the crystallinity of the film as projected by XRD analysis [27]. When Nd doping concentration is less, the nucleation of atoms gets reduced and the surface mobility becomes low for the deposited atoms. A sufficient doping material (5 at% Nd) needs to be provided for the atoms to coalesce and form larger grains on the substrates. Therefore, it is apparent that the Nd doping concentration has a reasonable effect on the surface smoothness and the size of grain of SnS films.

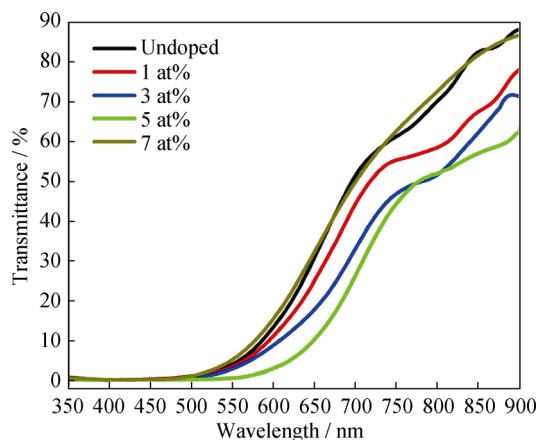
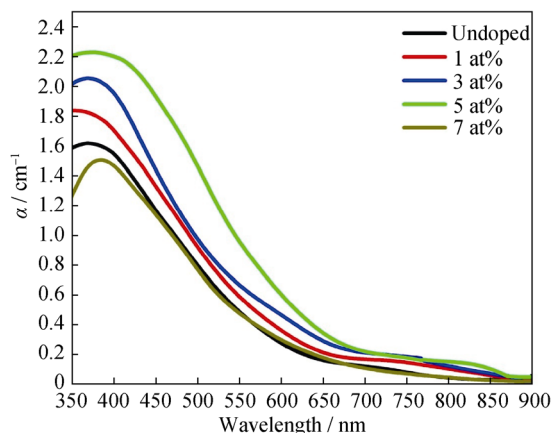
The chemical composition of SnS thin films prepared using NSP deposition was determined by EDX spectra. Figure 4a–e illustrates EDX spectra of the films deposited at 0 at% to 7 at% Nd doping concentration. The EDX spectra show Sn and S peaks along with Nd peaks, confirming the presence of tin (Sn), sulfur (S) and (Nd) neodymium in the samples, and the contents of these elements are given in Table 3. The atomic ratio of S/Sn is nearly stoichiometric in 0 at%–7 at% Nd-doped SnS films. It has been observed that upon increasing the Nd concentration, the content of Sn in the films decreases slightly, whereas the content of S is almost constant. It would be presumed that Nd doping in the films is substitutional. Additional peaks in EDX except Sn, S and Nd peaks are for O, Si from substrate and solvent of the precursor solution.

3.4 Optical properties

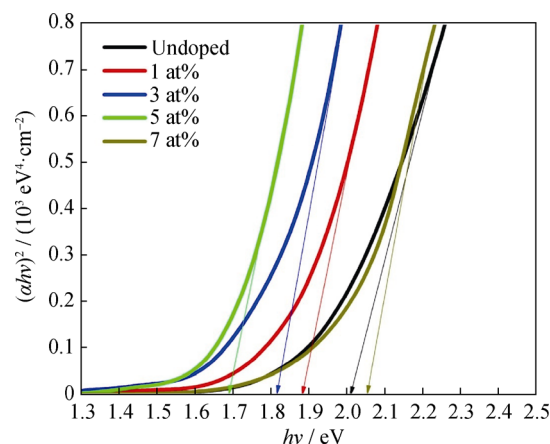
The wavelength (λ) versus transmittance (T) and absorption coefficient (α) plots of SnS thin films prepared with various Nd doping concentrations are seen in Figs. 5, 6. It is

Table 3 Elemental analysis of undoped and Nd-doped SnS thin films

Nd doping content/at%	Content/at%			Nd/Sn atomic ratio
	Sn	S	Nd	
0	50.98	49.02	0	–
1	49.78	49.58	0.64	1.28
3	48.48	49.77	1.75	3.61
5	47.32	49.62	3.06	6.47
7	46.21	48.64	5.15	11.14

**Fig. 5** Transmittance spectra of Nd:SnS films with different Nd doping contents**Fig. 6** Absorption coefficient spectra of Nd:SnS films with different Nd doping contents

observed from the plots that the optical transmittance of SnS films increases with the increase in incident wavelength but decreases with the increase in Nd doping concentration up to 5 at% beyond which it starts to increase. In the visible spectral region, reflection decreases during transmission which signifies that light is reduced due to scattering [33]. Therefore, the absorption edge of the Nd-

**Fig. 7** $(\alpha hv)^2$ vs hv of Nd:SnS films with different Nd doping contents

doped SnS thin films is shifted toward the higher wavelength (red shift). The lesser transmittance value of 5 at% Nd-doped SnS films signifies the absorption of light.

The absorption coefficient (α) was obtained using the equation as follows:

$$\alpha = \frac{\ln(1/T)}{t} \quad (7)$$

where t is film thickness and T is transmittance.

Absorption spectra obtained for the wavelength range of 350–900 nm is shown in Fig. 6, it demonstrates a notable rise in the absorption of the films fabricated with the Nd doping concentration increasing from 0 at% to 5 at%. For the further increase in Nd doping concentration (7 at%), the absorption of the film decreases. The optical bandgap (E_g) of the semiconductor thin films was evaluated [34] using Eq. (8).

$$(\alpha hv)^2 = A(hv - E_g) \quad (8)$$

where αhv is absorption coefficient in terms of energy, hv is photon energy and A is proportionality constant. The plot drawn between $(\alpha hv)^2$ and hv was used to find the energy bandgap value of the materials. The bandgap calculated from Fig. 7 shows a decrease from 2.05 to 1.69 eV with Nd doping content from 0 at% to 7 at%, as shown in Table 2. This decrease in bandgap indicates the improvement in crystallinity with the increase in Nd concentration, denoting a variation in localized density states in the energy gap. Also, the reduction in E_g may be from the band shrinkage effect occurred due to the enhancement in the level of charge carriers [34].

3.5 PL studies

Figure 8 shows the photoluminescence spectra of the films measured in the range of 400–900 nm using an excitation

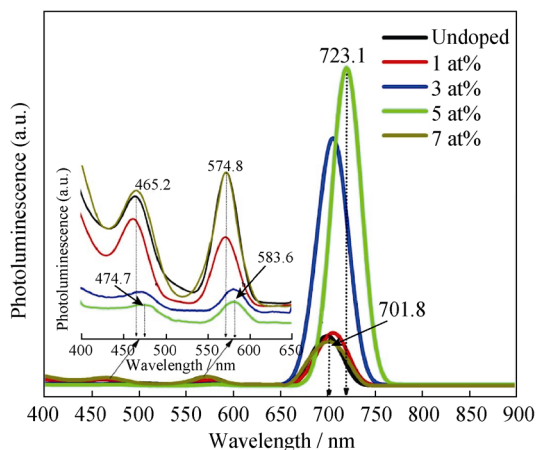


Fig. 8 PL spectra of undoped and Nd-doped SnS thin films with different Nd doping contents

of $\lambda_{exc} = 350$ nm. The intensity of prominent emission peak observed at 723.1 nm increases with the increase in Nd doping concentration up to 5 at% and then decreases for further doping level. The peak position is shifted along higher λ side related to pure SnS film, and intensity variations are attributed to the density of free excitons and concentration quenching mechanism. The E_g value obtained from UV-Vis spectra is low in comparison with the emission peak at 723.1 nm [35]. There are two additional minor peaks found for Nd-doped SnS films. The first major intense peak attributes to blue emission between 465.2 and 474.7 nm, and the second major peak is obtained for the yellow emission of 574.8 and 583.6 nm. The peak at 474.7 nm signifies S^- and Sn^+ vacancies with high density, as well as the impact of various imperfections such as interstitial, stacking faults [26]. The peak at 583.6 nm for yellow emission is associated with the crystal defects or impurities [36]. It has an agreement with the former reports of 760 nm for bulk SnS [37] and 725 nm for SnS films [38]. The Nd doping enlarges the band edge emission peak intensity which is strongly coherent with the XRD pattern for the increase in Nd doping concentration.

3.6 Electrical properties

Electric performance determines the suitability of films to use in solar cell applications, and those were studied through Hall effect. Variation in resistivity, mobility and concentrations of carriers with the change in Nd doping content is shown in Fig. 9. The electrical parameters recorded using the Hall effect measurements are tabulated in Table 4. All the films show p-type conductivity. Extremely improved electrical properties are observed for Nd-doped SnS thin films compared with undoped SnS thin film. The low resistivity, high Hall mobility and high carrier concentration are observed at 5 at% Nd-doped SnS

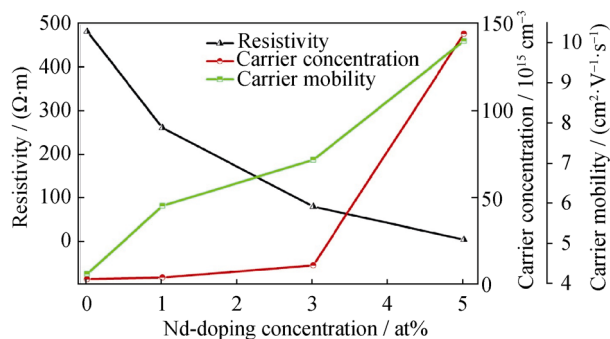


Fig. 9 Variation of resistivity, carrier concentration and mobility of undoped and Nd-doped SnS thin films

Table 4 Variation of resistivity, carrier concentration and mobility of Nd-doped SnS thin films

Nd doping content/at%	Resistivity/ ($\Omega\cdot\text{cm}$)	Carrier concentration/ cm^{-3}	Hall mobility($\text{cm}^2\cdot\text{V}^{-1}\cdot\text{s}^{-1}$)
0	4.818×10^2	3.052×10^{15}	4.245
1	2.612×10^2	4.021×10^{15}	5.943
3	7.981×10^1	1.103×10^{16}	7.090
5	4.311×10^0	1.441×10^{17}	10.048

film. The resistivity of prepared films decreases due to the replacement of divalent element by trivalent element in the host lattice site, and it leads to the increase in carrier concentration and Hall mobility. For a doping concentration of more than 5 at%, the resistivity again increases, while carrier concentration and Hall mobilities decrease. The same trend in the variation of carrier concentration and hole mobility is reported on bismuth doping [31] and Ag doping [34] in SnS films deposited using spray pyrolysis technique. There are two reasons for the increase in resistivity, i.e., lattice disorder and Nd which acts as surface acceptors on SnS surface and increases the Schottky barrier [34, 39]. From the analysis of the present work, the authors confirm that the optimum dopant concentration to get good electrical properties is 5 at%.

3.7 Photovoltaic (PV) studies

SnS-based PV cell was constructed using 5 at% Nd-doped SnS film with CdS layer on FTO substrate. The $I-V$ nature of the inverted FTO/n-CdS/p-Nd:SnS/Al device illuminated with a light source of $100 \text{ mW}\cdot\text{cm}^{-2}$ is revealed in Fig. 10. Dark $I-V$ (inset of Fig. 10) and illuminated $I-V$ solar cell curves are shown in Fig. 10. In the dark, it gives a minimum value of current which is attributed to the minority carriers. After illuminating, the current is raised due to the charge carriers produced by incident photons.

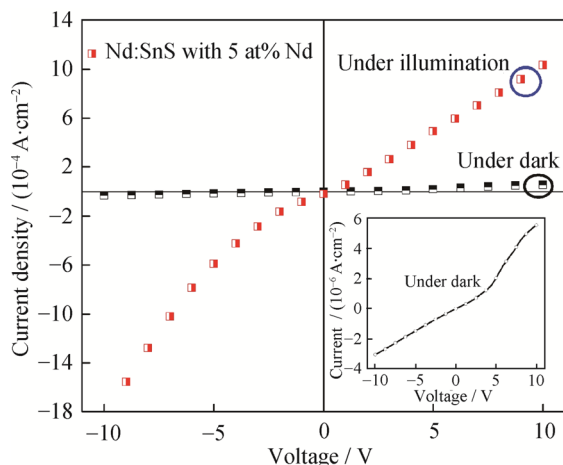


Fig. 10 *I-V* characteristics for FTO/CdS/Nd-SnS heterostructure films and inset being dark *I-V* characteristics of FTO/CdS/Nd-SnS heterostructure films

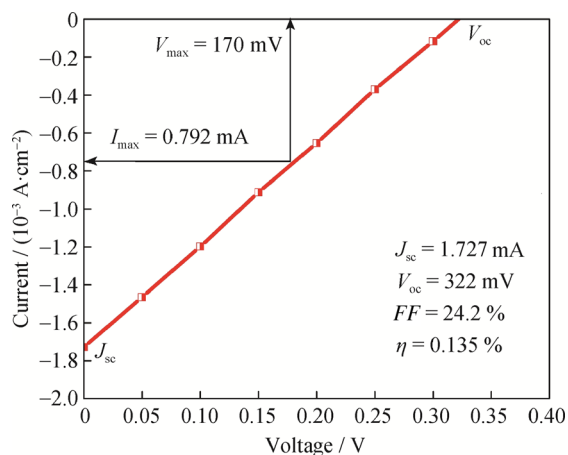


Fig. 11 Illuminated *I-V* characteristics of FTO/n-CdS/p-Nd:SnS heterostructure with 5 at% Nd under illumination

The forward current increases with applied voltage, while the reverse current shows very little increment. It confirms the formation of the p–n photoactive hetero-junction at the interface of CdS and Nd-SnS and is consistent with the p-type and n-type conductivities of Nd-SnS and CdS, respectively.

Under the illumination, the photocurrent is perceived and its characteristic curve is seen in Fig. 11 with regard to open-circuit voltage (V_{oc}) and short-circuit current (I_{sc}). A power conversion efficiency (η) of 0.135%, a V_{oc} of 322 mV and short-circuit current density (J_{sc}) of $1.727 \text{ mA}\cdot\text{cm}^{-2}$ are obtained for the doping of 5 at% Nd. The efficiency (η) was calculated using the following Eqs. (9) and (10):

$$FF = \frac{V_{max} I_{max}}{V_{oc} J_{sc}} \quad (9)$$

$$\eta = \frac{FF J_{sc} V_{oc}}{P_{in}} \quad (10)$$

Where FF is fill factor, J_{sc} is short circuit current density, V_{oc} is open circuit voltage, P_{in} is input power, V_{max} is maximum voltage and I_{max} is maximum current density. Though the device shows asymmetric level of currents both in forward and reverse, it shows a linear variation of current both in forward and reverse. This may be due to the formation of poor interface and thus p–n junction. Thus, the photovoltaic effect of the CdS/SnS cells through NSP is weaker than that of CdS/SnS cells by spray pyrolysis technique [38]. The major criteria for the low efficiency of the device are due to the various types of loss mechanisms involved during the processing of the film. The prepared SnS film mostly contains small grains which produced more grain boundaries, so there are more recombination sites for the minority carrier [40].

4 Conclusion

Influences of Nd doping concentration on structural, morphological, optoelectronic and photovoltaic characters of SnS films coated by NSP method were analyzed. XRD studies imparted the growth of polycrystalline films with (111) orientation and orthorhombic structure of films. Size of crystallites was improved from 17 to 41 nm depending upon the Nd concentration. Nd-doped SnS was clearly confirmed by Raman analysis. The surface roughness of the films increased from 7 to 32 nm with the increase in Nd concentration. The films showed transmittance value of more than 62% in the visible region, the energy gap (E_g) decreased from 2.05 to 1.69 eV by increasing the doping content. The PL measurements indicated a considerable red shift, since there was a modulation in the bandgap on Nd doping. The incorporation of Nd into SnS was confirmed from the electrical and optical studies also. The variation in electrical resistivity and reduction in the optical bandgap happened due to the successful incorporation of Nd^{3+} into SnS lattice site. At 5 at% Nd doping, the obtained low resistivity value was about $4.311 \Omega\cdot\text{cm}$, whereas a high carrier concentration was noticed. So, neodymium doping can alter the properties of the SnS thin films and can be used in optoelectronic applications.

Acknowledgements This work was financially supported by the project from the Department of Science and Technology, New Delhi, India (DST-SERB) (No.SB/FTP/PS-131/2013). Authors from KKU express their appreciation to the Deanship of Scientific Research at King Khalid University for funding this work through research groups program under grant number R.G.P. 2/42/40.

References

- [1] Noguchi Hidenori, Setiyadi Agus, Tanamura Hiromasa, Nagatomo Takao, Omoto Osamu. Characterization of vacuum-evaporated tin sulfide film for solar cell materials. *Sol Energy Mater Sol Cells*. 1994;35:325.
- [2] Avallaneda D, Delgado G, Nair MTS, Nair PK. Structural and chemical transformations in SnS thin films used in chemically deposited photovoltaic cells. *Thin Solid Films*. 2007;515(15):5771.
- [3] Parenteau Martin, Carlone Cosmo. Influence of temperature and pressure on the electronic transitions in SnS and SnSe semiconductors. *Phys Rev B Condens Matter*. 1990;41(8):5227.
- [4] Akkari A, Guasch C, Kamoun-Turki N. Chemically deposited tin sulphide. *J Alloy Compd*. 2010;490(1–2):180.
- [5] Ray SC, Karanjai MK, Gupta DD. Structure and photoconductive properties of dip-deposited SnS and SnS₂ thin films and their conversion to tin dioxide by annealing in air. *Thin Solid Films*. 1999;350(1):72.
- [6] Wei GP, Zhang ZL, Zhao WM, Gao XH, Chen WQ, Tanamura H, Yamaguchi M, Noguchi H, Nagatomo T, Omoto O. Investigation on SnS film by RF sputtering for photovoltaic application. In: *Proceedings of IEEE 1st world conference on photovoltaic energy conversion part 2*. Waikoloa, HI, USA; 1994. 365.
- [7] Kumar KDA, Valanarasu S, Tamilnayagam V, Amalraj L. Structural, morphological and optical properties of SnS₂ thin films by nebulized spray pyrolysis technique. *J Mater Sci Mater Electron*. 2017;28(19):14209.
- [8] Lokhande BJ, Patil PS, Uplane MD. Studies on structural, optical and electrical properties of boron doped zinc oxide films prepared by spray pyrolysis technique. *Phys B*. 2001;302:59.
- [9] Ge YH, Guo YY, Shi WM, Qiu YH, Wei GP. Influence of In-doping on resistivity of chemical bath deposited SnS films. *J Shanghai Univ*. 2007;11(4):403.
- [10] Stavrinadis A, Smith JM, Cattley CA, Cook AG, Grant PS, Watt AAR. SnS/PbS nanocrystal heterojunction photovoltaics. *J Nanotechnol*. 2010;21(18):185202.
- [11] Zhang S, Chen SY, Jia HJ, Zhou HF. Preparation and characterization of aluminium-doped SnS thin films. *Adv Mater Res*. 2012;418–420:712.
- [12] Jamali-Sheini F, Niknia F, Cheraghizade M, Yousefi R, Mahmouadian MR. Broad spectral response of Se-doped SnS nanorods synthesized through electrodeposition. *Chem Electro Chem*. 2017;4(6):1478.
- [13] Dussan Cuenca A, Mesa F, Gordillo G. Effect of substitution of Sn for Bi on structural and electrical transport properties of SnS thin films. *J Mater Sci*. 2001;45(9):2403.
- [14] Reghima M, Akkari A, Guasch C, Kamoun NT. Synthesis and characterization of Fe-doped SnS thin films by chemical bath deposition technique for solar cells applications. *J Mater Sci*. 2012;47(3):1365.
- [15] Reghima M, Akkari A, Guasch Cathy, Kamoun NT. Structural, optical, and electrical properties of SnS: Ag thin films. *J Electron Mater*. 2015;44(11):4392.
- [16] Urbaniak A, Pawlowski M, Marzantowicz M, Sall T, Marí B. Opto-electrical characterisation of In-doped SnS thin films for photovoltaic applications. *Thin Solid Films*. 2017;636:158.
- [17] Santhosh Kumar K, Gowri Manohari A, Lou C, Mahalingam T, Dhanapandian S. Influence of Cu dopant on the optical and electrical properties of spray deposited tin sulphide thin films. *Vacuum*. 2016;128:226.
- [18] Sajeesh TH, Jinesh KB, Sudha Kartha C, Vijayakumar KP. Role of pH of precursor solution in taming the material properties of spray pyrolysed SnS thin films. *Appl Surf Sci*. 2012;258(18):6870.
- [19] Ristov M, Sinadinovski G, Mitreski M, Ristova M. Photovoltaic cells based on chemically deposited p-type SnS. *Sol Energy Mater Sol Cells*. 2001;69(1):17.
- [20] Kafashan Hosein, Ebrahimi-Kahrizsangi Reza, Jamali-Sheini Farid, Yousefi Ramin. Effect of Al doping on the structural and optical properties of electrodeposited SnS thin films. *Phys Status Solidi A*. 2016;213(5):1302.
- [21] Bommireddy PR, Musalikunta CS, Uppala C, Park SH. Influence of Cu doping on physical properties of sol-gel processed SnS thin films. *Mater Sci Semicond Process*. 2017;71:139.
- [22] Kumar KDA, Valanarasu S, Jeyadheepan K, Kim HS, Vikraman D. Evaluation of the physical, optical, and electrical properties of SnO₂: F thin films prepared by nebulized spray pyrolysis for optoelectronics. *J Mater Sci Mater Electron*. 2018;29(5):3648.
- [23] Bokare A, Sanap A, Pai M, Sabharwal S, Athawale AA. Antibacterial activities of Nd doped and Ag coated TiO₂ nanoparticles under solar light irradiation. *Colloids Surf B Bio Interfaces*. 2013;102:273.
- [24] Wojcieszak D, Mazur M, Kurnatowska M, Kaczmarek D, Domaradzki J, Kepinski L, Chojnacki K. Influence of Nd-doping on photocatalytic properties of TiO₂ nanoparticles and thin film coatings. *Int J Photo Energy*. 2014. <https://doi.org/10.1155/2014/463034>.
- [25] Niknia Farhad, Jamali-Sheini Farid, Yousefi Ramin. Photocurrent properties of undoped and Pb-doped SnS nanostructures grown using electrodeposition method. *J Electron Mater*. 2015;44(12):4734.
- [26] Nikolic PM, Miljkovic L, Mihajlovic P, Lavrencic B. Splitting and coupling of lattice modes in the layer compound SnS. *J Phys C Solid State Phys*. 1977;10(11):289.
- [27] Srinivasa Reddy T, Santhosh Kumar MC. Co-evaporated SnS thin films for visible light photodetector applications. *RSC Adv*. 2016;6(96):95680.
- [28] Chandrasekhar HR, Humphreys RG, Zwick U, Cardona M. Infrared and Raman spectra of the IV–VI compounds SnS and SnSe. *Phys Rev B*. 1977;15(4):2177.
- [29] Chandrasekhar HR, Zwick U. Raman scattering and infrared reflectivity in GeSe. *Solid State Commun*. 1976;18(11–12):1509.
- [30] Srinivasa Reddy T, Santhosh Kumar MC. Effect of substrate temperature on the physical properties of co-evaporated Sn₂S₃ thin films. *Ceram Int*. 2016;42(10):12262.
- [31] Mahalingam T, Gowri Manohari A, Dhanapandian S, Santhosh K. Effect of doping concentration on the properties of bismuth doped tin sulfide thin films prepared by spray pyrolysis. *Mater Sci Semicond Process*. 2014;17:138.
- [32] Santhosh Kumar K, Manoharan C, Dhanapandian S, Gowri Manohari A. Effect of Sb dopant on the structural, optical and electrical properties of SnS thin films by spray pyrolysis technique. *Spectrochim Acta Part A Mol Biomol Spectrosc*. 2013;115:840.
- [33] Selim MS, Gouda ME, El-Shaarawy MG, Salem AM, Abd El-Ghany WA. Effect of thickness on optical properties of thermally evaporated SnS films. *Thin Solid Films*. 2013;527:164.
- [34] Santhosh Kumar K, Gowri Manohari A, Dhanapandian S, Mahalingam T. Physical properties of spray pyrolyzed Ag-doped SnS thin films for opto-electronic applications. *Mater Lett*. 2014;131:167.
- [35] Santhosh Kumar K, Manoharan C, Dhanapandian S, Gowri Manohari A, Mahalingam T. Effect of indium incorporation on properties of SnS thin films prepared by spray pyrolysis. *Opt Int J Light Electron Opt*. 2014;125(15):3996.

- [36] Sohila S, Rajalakshmi M, Chanchal Ghosh AK, Arora C Muthamizhchelvan. Optical and Raman scattering studies on SnS nanoparticles. *J Alloys Compd.* 2011;509(19):5843.
- [37] Sreedevi G, Reddy VRM, Park C, Chan-Wook J, Ramakrishna Reddy KT. Comprehensive optical studies on SnS layers synthesized by chemical bath deposition. *Opt Mater.* 2015;42:468.
- [38] Arulanantham AMS, Valanarasu S, Kathalingam A, Jeyadheepan K. Solution volume effect on structural, optical and photovoltaic properties of nebulizer spray deposited SnS thin films. *J Mater Sci Mater Electron.* 2018;29(15):12899.
- [39] Joseph B, Manoj PK, Vaidyan VK. Studies on the structural, electrical and optical properties of Al-doped ZnO thin films prepared by chemical spray deposition. *Ceram Int.* 2006;32(5):487.
- [40] Ghosh Biswajit, Das Madhumita, Banerjee Pushan, Das Subrata. Fabrication of the SnS/ZnO heterojunction for PV applications using electrodeposited ZnO films. *Semicond Sci Technol.* 2009; 24(2):025024.